Preparation and Properties of Polyamide 6/Polypropylene–Vermiculite Nanocomposite/Polyamide 6 Alloys

S. C. Tjong,[1] Y. Z. Meng,[1,2] Y. Xu[2]

[1] *Department of Physics & Materials Science, City University of Hong Kong, 83 Tat Chee Avenue, Kowloon, Hong Kong*
[2] *Guangzhou Institute of Chemistry, Chinese Academy of Sciences, P.O. Box 1122, Guangzhou 510650, People's Republic of China*

Received 29 November 2001; accepted 3 February 2002

ABSTRACT: Polypropylene–vermiculite nanocomposites can be achieved by simple melt mixing of maleic anhydride-modified vermiculite with polypropylene. Maleic anhydride acts either as a compatibilizer for the polymeric matrix or as a swelling agent for the silicate. Compatibilized blends are injection molded directly from polyamide 6 and polypropylene–vermiculite nanocomposites. Scanning electron microscopy observation reveals that a two-phase structure consisting of polypropylene–vermiculite nanocomposite and polyamide 6 is formed in the blends. The absence of vermiculite reflections in the X-ray powder diffraction patterns indicates that the polypropylene–vermiculite phase exhibits nanocomposite characteristics. Tensile test shows that the tensile modulus of the polymer alloy tends to increase with increasing polypropylene–vermiculite nanocomposite content. The tensile strength of composite containing 8 wt % vermiculite is higher than that of pure polyamide 6. Finally, the thermal properties of the nanocomposites are determined by dynamic mechanical analysis, differential scanning calorimetry, and thermogravimetric measurements. The effects of maleic anhydride addition on the formation of polypropylene–vermiculite nanocomposite reinforcement and on the mechanical properties of composites are discussed. © 2002 Wiley Periodicals, Inc. J Appl Polym Sci 86: 2330–2337, 2002

Key words: polyamide; nanocomposite; vermiculite; maleic anhydride; exfoliation

INTRODUCTION

Polyamide 6 (PA6) is used in a wide range of engineering applications because of its unique mechanical properties and processability. To further upgrade the performance of PA6, various reinforcements (e.g., glass, carbon, natural fiber, and whiskers) are often incorporated into polyamides.[1,2] Recently increasing attention is being directed toward the fabrication of *in situ* nanocomposites with silicate reinforcements.[3] Nanocomposites exhibit a markedly improved mechanical properties because of their nanometer scale dispersion of reinforcements and their high surface-to-volume ratio.[4] Silicates, such as montmorillonite, hetorite, and mosco-clay, have been frequently used as reinforcing fillers for the polymers because of their potentially high aspect ratios.[4] These silicates exhibit a layered structure of ~1-nm thickness when they are properly exfoliated. The layered platelets are very stiff, thus have very high strength. Accordingly, it is advantageous to develop polyamide nanocomposites using low loading levels of silicates.

Correspondence to: S. C. Tjong (aptjong@cityu.edu.hk).

Journal of Applied Polymer Science, Vol. 86, 2330–2337 (2002)

Layered silicates are able to undergo cation-exchange reactions. To achieve a nanoscale dispersion of silicates in polyamides, the silicates are generally pretreated with alkyl ammonium ions that exchange inorganic cations of the clays.[5] Polyamide nanocomposites can be prepared either by mixing such organosilicates with the monomers followed by polycondensation or by melt mixing the organosilicates with polymer.[6–8] The pretreated organoclays can then be easily dispersed in a polymer matrix, forming nanocomposites with intercalated or exfoliated structure. In the former case, the spacing between the silicate layers is increased, which is associated with the incorporation of extended polymer chains into the layers. In exfoliated structure, extensive polymer chains penetrate into the galleries of the clays, resulting in total delamination of the silicate layer. Generally, melt compounding of high molecular weight polymers with organosilicates is difficult to afford nanocomposites with exfoliated structure because long molecular chains are less likely to diffuse into the galleries of silicates. More recently, Kim et al. have fabricated polyamide–silicate nanocomposites via direct polymer melt intercalation in which the polymer chains are diffused into the silicate galleries.[9] Such an approach to prepare nanocomposites shows promising commercial applications. Little information is available in the literature concerning the nanocompos-

TABLE I
Composition and Properties of Vermiculite

Particle size, mesh	Surface area, m^2/g	SiO_2	Al_2O_3	MgO	Fe_2O_3	CaO	K_2O	C
<10	<1	45%	9%	21.5%	6%	5%	1%	0.2%

ites preparation via direct melt blending. Moreover, the mechanism of nanostructure formation remains unclear.[10–13]

In previous studies, we prepared maleic anhydride (MA)-grafted polypropylene (MPP) macrocomposites reinforced with various fiber reinforcements in a twin-screw extruder followed by injection molding.[14–17] MA can be readily melt grafted onto PP chains, thereby improving the affinity between resulting MPP and various inorganic reinforcements. In more recent work,[3c] we introduced MA into the vermiculite galleries to produce MA-intercalated vermiculite (MAV) by the solution treatment method. Accordingly, PP can be melt blended with MAV to form a ternary molecular structure of vermiculite–MA–PP in the presence of dicumyl peroxide (DCP). In such a structure, MA acts as a bridge to bond the vermiculite and PP together. Therefore, vermiculite–PP nanocomposites with exfoliated structure can be prepared by simple melt mixing from MAV and PP.

In this paper, we attempt to develop a new procedure to fabricate composites based on PA6 and the PP–MAV nanocomposite. Possible interactions between PP–MAV nanocomposite and PA6 via MA are investigated. The main purpose is to examine the morphology, mechanical properties, and thermal properties of PA6/(PP–MAV) nanocomposite alloys and to correlate the relationships between these properties and microstructure.

EXPERIMENTAL

Materials

The vermiculite used in this work was purchased from Aldrich with grade number 3. Its physical and chemical properties are tabulated in Table I. The polypropylene (Profax 6331) with a melt flow index of 12 g/10 min was purchased from Himont Company. Russian-made PA6 pellets (PA6-120/321) were used as matrix material of composites. The PA6 has a molecular weight (M_w) of 56,000 and a density of 1.13 g cm^{-3}. MA supplied by Fluka Chemie, and DCP produced by Aldrich Chemical Company were used as received for the maleation of PP or exfoliation of vermiculite. Other reagent grade chemicals were also used without further treatment.

Organo-vermiculite preparation

The vermiculite was first pretreated with hydrochloric acid according to a reported patent.[18] To a 2.0-L polypropylene beaker containing 1 L of 2 M HCl, 25 g of the preground vermiculite was introduced at room temperature. The resulted dispersion solution was magnetically stirred for 8 h. The pH of the resulting slurry was then adjusted to /3.0–4.0. Upon filtering, the vermiculite was washed thoroughly with distilled water several times until the filtrate had a pH value of 7.0. Following washing, the resulting solid was dried at 160 °C overnight. The final ground product was a fine powder with original color. The acid-delaminated vermiculite was then further treated with maleic anhydride to prepare MAV. To a 500-mL polypropylene beaker, 17.4 g of MA, 156.6 g of acid-treated vermiculite, and 250 mL of acetic acid were added. The mixture was ultrasonically stirred for 2 h to ensure MA entering the galleries of acid-delaminated vermiculite. The resulting slurry was dried in a rotavapor at 60 °C, and subsequently dried at 70 °C for 24 h under vacuum. The final MAV in the form of fine powder was kept in a dryer.

Preparation of pp–mav nanocomposite/pa6 alloys

According to previous work,3c the PP–MAV (2.5/1.0, w/w) nanocomposite was prepared in a twin-screw Brabender Plasticorder at 15–35 rpm by a one-step reaction of PP with MAV in the presence of DCP. The blending temperature profile was 200 — 220 — 230 — 180 °C. The weight ratio of PP, MAV, and DCP was fixed at 434:174:0.5. The extrudates were pelletized on exiting the pelletizer from the extruder. Subsequently, the PA6/(PP–MAV) ternary composites were directly fabricated in the same twin-screw extruder from the PP–MAV (2.5/1.0, w/w) nanocomposite and PA6. The process was performed by a one-step reaction at a temperature profile of 220 — 240 — 240 — 200 °C at 30 rpm. The extrudates were also pelletized on exiting the pelletizer and they were dried in an oven for 8 h at 100 °C prior to injection molding. Finally, the PA6/PP–MAV pellets were directly injection molded into standard dog-bone tensile bars (ASTM D638). The mold temperature was maintained at 40 °C, whereas the barrel zone temperatures were set at 230, 240, and 240 °C. An injection pressure of 70 bar and a holding pressure of 40 bar were selected.

Torque measurements

Torque values for the PP–MAV (2.5/1.0, w/w) nanocomposite and pure PA6 were measured with a Bra-

bender Plasticorder batch mixer at 240 °C at 35 rpm for 5 min. The chamber volume was 50 cm^3. For each examination, 35 g of material was added into the batch.

Mechanical measurements

The tensile behavior of the PA6/(PP–MAV) nanocomposite alloys was examined with an Instron tensile tester (model 4206) at a conditioned temperature of 23 °C. The cross-head speed was set at 5 mm min^{-1}. Seven specimens of each composition were tested, and the average values are reported.

Dynamic mechanical analysis (DMA) of the injection-molded composites was performed with a DuPont dynamic mechanical analyzer (model 983) at a fixed frequency of 1 Hz and an oscillation amplitude of 0.2 mm. The temperature studied ranged from −30 to 170 °C, with a heating rate of 2 °C min^{-1}.

Morphological observations

The injection molded tensile bars were fractured in liquid nitrogen. The morphology of specimens was examined by transmission electron microscope (TEM; Philips CM20) and field emission scanning electron microscope (SEM; JEOL JSM model 6335F). For TEM examination, ultrathin specimens (~50 nm) were cut from the middle section of injection-molded bars, parallel to the flow direction. Cutting operations were carried out with a Reichert Ultracut microtome under cryogenic conditions, and the film was retrieved onto Cu grids. The thin films were stained for 10 h in OsO_4 solution, followed by coating with a very thin layer of carbon (~5 nm) prior to TEM examination.

Thermal analyses

The 5% weight loss temperatures of the composites were determined with a Seiko thermogravimetric analyzer (TGA; model SSC-5200) from 30 to 600 °C under a protective helium atmosphere (200 mL/min). The heating rate was 20 °C min^{-1}. The glass transition temperatures (T_gs) were determined with Perkin-Elmer 7C DSC instrument at a heating rate of 20 °C/min under nitrogen flow.

X-ray diffraction analyses

X-ray diffraction patterns of composite powders were obtained with a Rigaku RINT X-ray diffractometer (model DMAX 1200) with Ni-filtered Cu Kα radiation. The patterns were recorded in the reflection mode 2θ = 1.5–15°, using a scanning speed and step size of 2° and 0.05°, respectively.

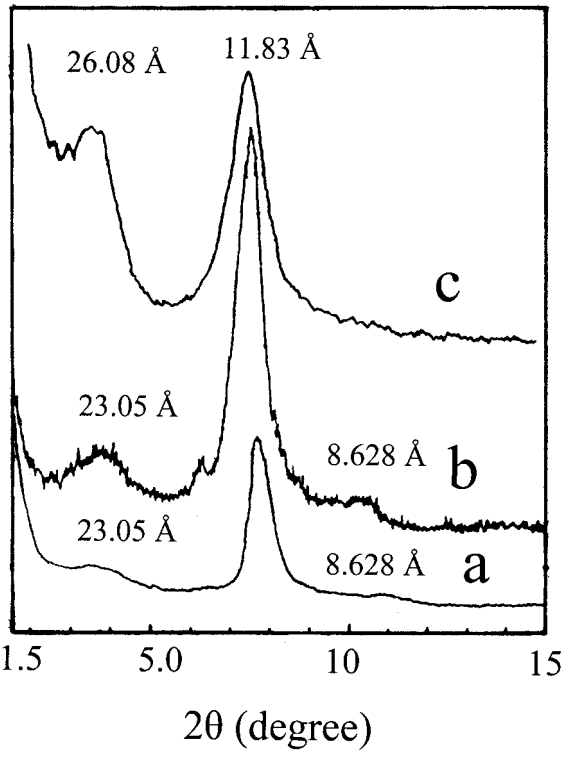

Figure 1 XRD patterns of vermiculite (a) as received without any treatment; (b) on heating for 24 h at 160 °C; and (c) acid delaminated by treatment with 2 M HCl followed by drying at 160 °C overnight.

RESULTS AND DISCUSSION

Maleic anhydride-delaminated vermiculite

Layered silicate-like vermiculite consists of two basic units; that is, tetrahedral and octahedral sheets. Within this structure, hydroxyl or fluoride ions are located at two octahedral corners. A composite sheet in this form is electrically neutral, and van der Waals-type forces are considered to bond the sheets together. Various methods have been tried for the delamination of vermiculite; for example, by pretreating vermiculite with a surfactant (e.g., alkyl ammonium ions) or reactive organic compounds to produce an organoclay,4b,[19] or via ion-exchange with concentrated lithium nitrate solution,[20,21] or by direct heating in a reactive vapor phase.[22]

In this work, an acid treatment route is used to delaminate the vermiculite. The X-ray diffraction patterns of vermiculite prior to and after acid treatments are shown in Figure 1. Untreated vermiculite exhibits characteristic (001) diffraction peaks at 3.833, 7.484, and 10.286°. These peaks correspond to the interlayer platelet spacings of 23.05, 11.83, and 8.628 Å (XRD pattern a of Figure 1), respectively. From the integrated results of XRD peak intensity, the vermiculite contains ~6.4 wt % fraction with an expanded spacing of 23.05 Å. After the vermiculite was dried at 160 °C

TABLE II
Mechanical Properties of (PP–MAV/PA6 Nanocomposite) Ternary Composites

Composites PA6/(PP-MAV)	Vermiculite content, wt %	Tensile strength, MPa	Tensile modulus, MPa	Storage modulus, GPa[a]	Elongation at break, %	Energy at break, *J*
Neat PA6	0	48.75	995.5	1.501	186.2	202.2
92.8%PA6/7.8%(PP–MAV)	2	47.17	1048.7	2.328	70.37	71.77
84.5%PA6/15.5%(PP–MAV)	4	47.45	1155.0	2.630	45.07	43.62
76.7%PA6/23.3%(PP–MAV)	6	47.22	1266.7	2.671	14.44	11.81
69.0%PA6/31.0%(PP–MAV)	8	50.20	1397.1	2.815	9.014	6.278

[a] Obtained from DMA analyses at 25 °C.

(XRD pattern b of Figure 1), the expanded vermiculite formed contains ~9.6 wt % fraction with 23.05 Å spacing. This result is 3.2% higher than that of the as-received sample, indicating that hydrated silicate could be partially delaminated by the thermal treatment. When the vermiculite was treated with 2 M HCl for 8 h, the diffraction peak with a spacing of 23.05 Å is broadened and shifted to 26.08 Å. Such a spacing is 3.03 Å larger than that of original vermiculite (Figure 1c), indicating the galleries of vermiculite are further separated.

To further delaminate the vermiculite, partially delaminated vermiculite was treated in a mixed MA and acetic acid solution by ultrasonic stirring. The XRD trace of the MAV exhibited no diffraction peaks, which is same result as in a previous work.[3c] This result implies that MA can readily enter the galleries of acid-treated vermiculite because acetic acid may act as a carrier to transport MA into vermiculite. Moreover, no characteristic peaks from 1.5 to 10° were observed in the XRD patterns of extruded PP–MAV nanocomposite (as shown in previous work 3c), indicating that vermiculite was completely intercalated or exfoliated.

Mechanical properties

The mechanical properties of PP–MAV/PA6 with vermiculite contents from 2 to 8% are summarized in Table II. The tensile strengths of composites remain nearly unchanged with increasing vermiculite contents up to ~6 wt %. At 8 wt % vermiculite, the 69% PA6/31.0% PP–MAV exhibits a higher tensile strength than neat PA6. Because PP exhibits a lower tensile strength than PA6,[23] it is considered that the vermiculite alone acts as the reinforcement for PA6/(PP–MAV), implying its good dispersion within the polymer matrices. The enhancement is considered to be an improvement of the compatibility between the vermiculite, PA, and PP associated with the MA addition. In other words, grafting reactions between MAV, PP, and PA6 are responsible for the compatibilizing effect of PA6/(PP–MAV) nanocomposite alloys. A schematic picture of the typical reactions is depicted in Figure 2.

It is noted from Table II that the tensile modulus, particularly the storage modulus, increases considerably with the reinforcement of PP–MAV nanocomposites. The elongation and energy at break, however, decrease greatly with the addition of the PP–MAV nanocomposite. The reduction in tensile ductility with increasing vermiculite content is a typical characteristic of discontinuous fiber-reinforced polymeric composites.[24]

The variation of storage modulus of composites versus vermiculite content is shown in Figure 3. The storage modulus increases dramatically with the increase in vermiculite content. The storage modulus of the composite with only 2% vermiculite is 2.328 GPa at

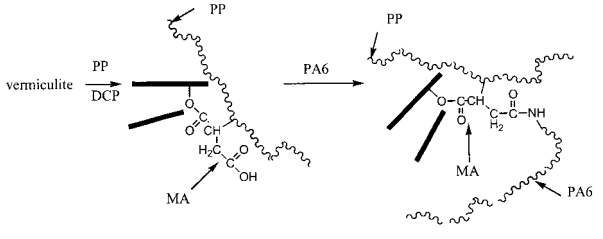

Figure 2 Artificial molecular structure of PA/(PP–MAV nanocomposite) ternary composite.

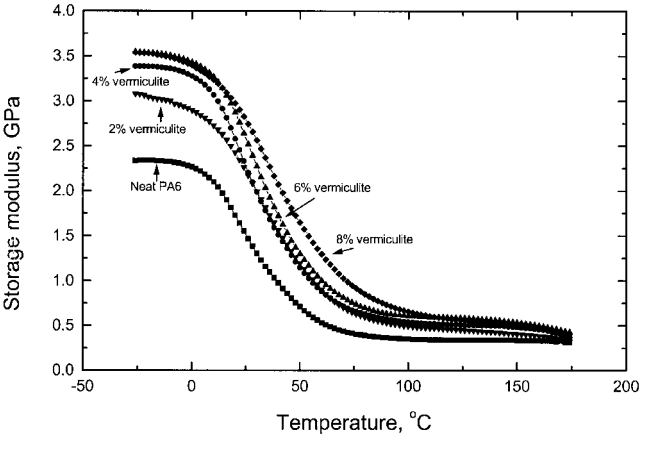

Figure 3 Storage modulus versus temperature for neat PA6 and PA/(PP–MAV) ternary composites.

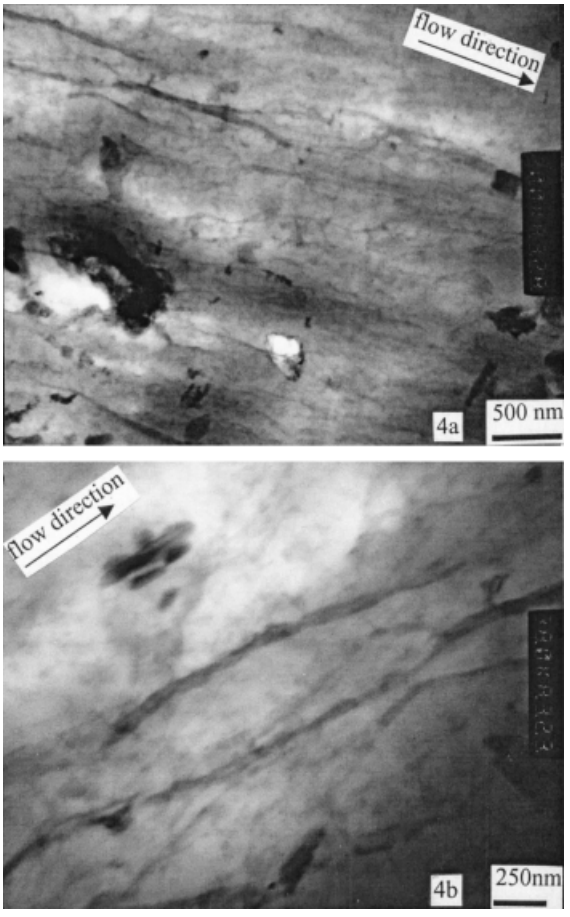

Figure 4 Typical TEM micrographs of PP–MAV (2.5/1.0, w/w) nanocomposite showing (a) formation of intercalated or exfoliated vermiculite layers in the composite, and (b) enlarged image of exfoliated vermiculite layers.

25 °C, which is 80% higher than that of neat PA6 (1.501 GPa). Generally, a synergistic reinforcing effect can occur between the silicate nanoscale layers and other macroscale reinforcements. Thus, melt compounding of PA6 with PP–MAV appears to be very effective for improving the mechanical properties of the ternary composites.

Microstructure of ternary composites

The TEM images of PP–MAV (2.5/1.0 w/w) binary nanocomposite prepared by *in situ* melt compounding are shown in Figures 4 a and b. The vermiculite, visible in black shadow, is oriented into fine layers that are parallel to the melt flow direction (Figure 4a). In the higher magnification TEM image of the nanocomposite (Figure 4b), intercalated or exfoliated vermiculite layers appear as dark-gray lines, and some clusters or stacks of the vermiculite are observed as thick dark lines along the melt flow direction (Figure 4a). These clusters or stacks exhibit a ribbon-like fibrillar morphology. These TEM micrographs show a similar morphology as those in a previous work,[3c] where the vermiculite contents of nanocomposites were relatively low. From Figure 4b, the vermiculite layer exhibits a length of ≥200 nm and therefore has a very large aspect ratio.

The SEM micrographs of the 92.8% PA6/7.8% PP–MAV and 84.5% PA6/15.5% PP–MAV nanocomposite alloys are shown in Figures 5a and 5b, respectively. Apparently, the ternary 92.8% PA6/7.8% PP–MAV composite with 2% vermiculite shows a two-phase microstructure that consists of the PP–MAV binary nanocomposite and PA6 matrix (Figure 5a). These rigid PP–MAV particles uniformly disperse within the PA6 matrix, hence dramatically reinforcing PA6. A similar morphology is observed for the 84.5% PA6/15.5% PP–MAV with 4% vermiculite (Figure 5b), with the exception that the dispersed particles are larger than those of Figure 5a. This difference is because the latter blend contains more of the PP–MAV nanocomposite component. This result illustrates that the large difference in melt viscosities between binary PP–MAV nanocomposites and the PA6 matrix during blending

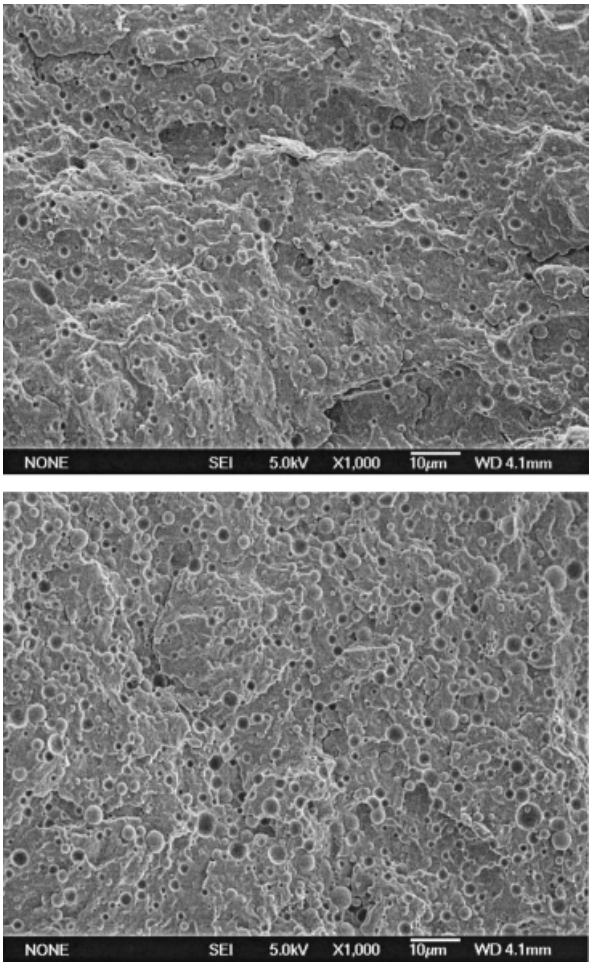

Figure 5 SEM micrographs of a (a) 92.8% PA6/7.8% (PP–MAV) composite and (b) 84.5% PA6/15.5% (PP–MAV) composite showing formation of PP–MAV spherical domains within the PA6 matrix.

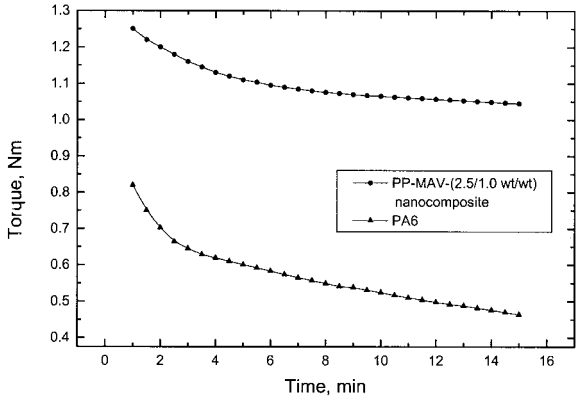

Figure 6 Torque versus mixing time for (a) PA6 and (b) PP–MAV (2.5/1.0, w/w) nanocomposite.

is responsible for the formation of the aforementioned two-phase system. The relationships between the torque and mixing time for PA6 and PP–MAV (2.5/1.0 w/w) binary nanocomposite are shown in Figure 6. It is apparent that the torque value of the PP–MAV binary nanocomposite is much higher than that of PA6. The high melt viscosity resulted from the high vermiculite content for the PP–MAV nanocomposite.

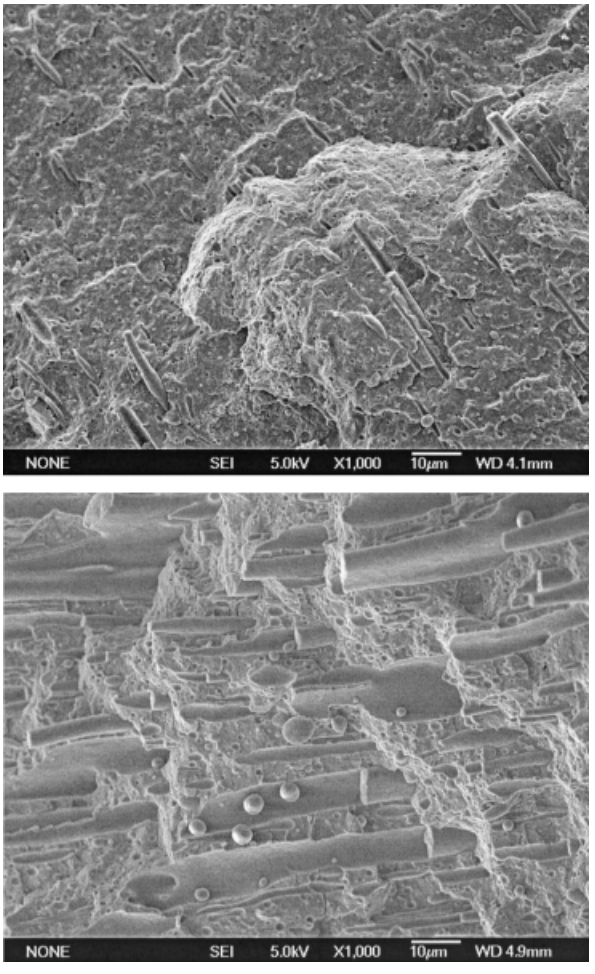

Figure 7 SEM micrographs of (a) 76.7% PA6/23.3% (PP–MAV) composite with elongated PP–MAV ellipsoids, and (b) 69.0% PA6/31.0% (PP–MAV) composite with PP–MAV fibrils within the PA6 matrix.

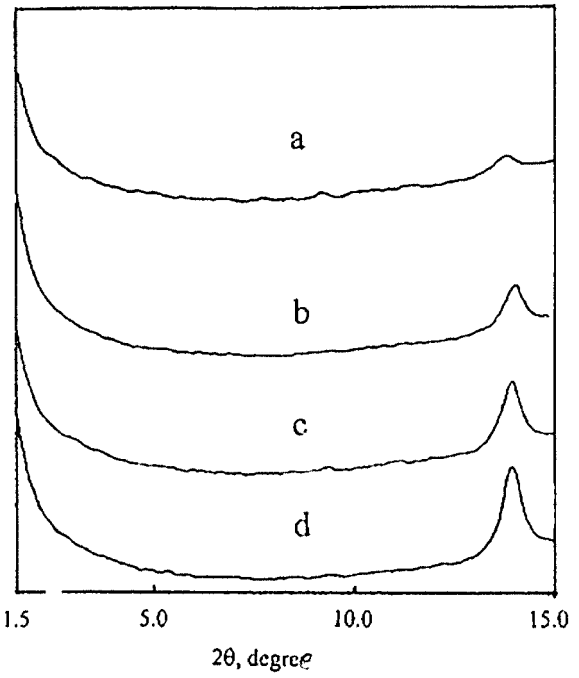

Figure 8 X-ray powder diffraction patterns for the PA6/(PP–MAV) nanocomposites formed in the twin-screw extruder: (a) 92.8% PA6/7.8% (PP–MAV) composite; (b) 84.5% PA6/15.5% (PP–MAV) composite; (c) 76.7% PA6/23.3%(PP–MAV) composite; (d) 69.0% PA6/31.0% (PP–MAV) composite.

The SEM micrographs of the fracture surfaces of the injection-molded 23.3% PP–MAV/76.7% PA6 and 31.0% PP–MAV/69.0% PA6 samples are shown in Figures 7a and 7b, respectively. The binary PP–MAV nanocomposite phase appears as elongated ellipsoids in the 76.7% PA6/23.3% PP–MAV nanocomposite alloy (Figure 7a), but as fibrils in the 69.0% PA6/31.0% PP–MAV (Figure 7b). Higher PP–MAV content favors the fibril creation within the PA6 matrix because the PP–MAV ellipsoids can be easily deformed into fibrillar morphology. From these SEM micrographs, it can be clearly seen that the fibrils have a large aspect ratio, although the diameters of the fibrils are rather large. The improved mechanical properties at 8 wt % vermiculite are mainly attributed to the formatiof of fibrils of the suspended PP–MAV phase (Table II).

As explored in previous work,[3c] MA-delaminated vermiculite can be well dispersed within PP at the nanoscale because of the associated shear forces within the extruder and the evaporation of MA during melt compounding. The XRD patterns of injection-molded PA6/(PP–MAV) nanocomposite alloys are shown in Figure 8. It is evident that there are no characteristic peaks from 1.5 to 10°, indicating that all

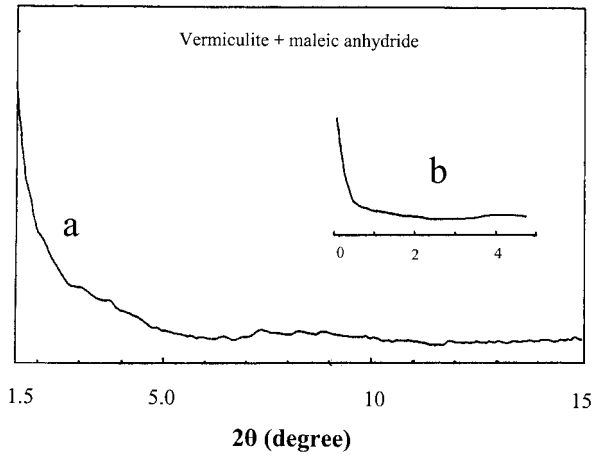

Figure 9 XRD patterns of MAV recorded with (a) wide angle ranging from 1.5 to 15°, and (b) small angle ranging from 0 to 5°.

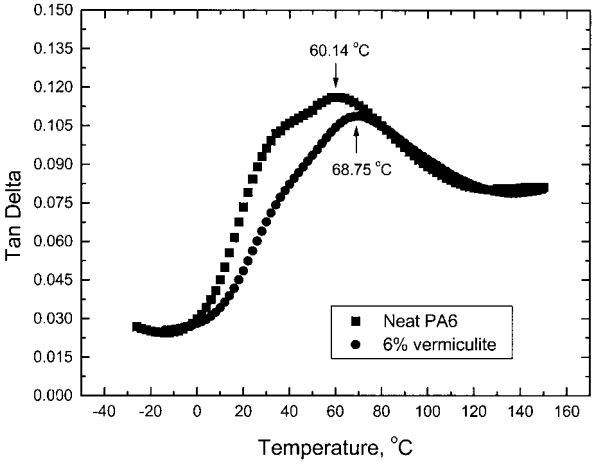

Figure 10 Loss modulus versus temperature for PA6 and 76.7% PA6/23.3% (PP–MAV) composite.

nanocomposites are intercalated or exfoliated. However, the intercalated or exfoliated vermiculite merely exist within the PP–MAV phase (Figure 9) because of the two-phase microstructure of PA6/(PP–MAV) nanocomposite alloys.

Thermal properties

The glass transition temperatures (T_g) of the composites obtained from the DMA tests are summarized in Table III. It can be seen that the introduction of PP–MAV nanocomposite results in an increase of the T_g of PA6 matrix from 60.14 to 68.75 °C. Cho and Paul[3b], reported that the presence of nanoscale particle does not affect the T_g of the PA6 matrix, but the crystalline melting points (T_ms) of the composites are lower than that of PA6. For PA6/(PP–MAV) ternary composites, blending of rigid PP–MAV nanocomposites with PA6 leads to an increase in T_g of ternary composites. The T_m of the PP tends to increase, whereas the T_m of the PA6 tends to decrease slightly. Consequently, the ($T_m^{PA} - T_m^{PP}$) value decreases with the increase of PP–MAV nanocomposite content, indicating an improvement in the compatibility between the PP–MAV and PA6 matrix. MPP acts as a compatibilizer between the PP–vermiculite phase and the PA6 matrix.

The loss modulus versus temperature for PA6 and 76.7% PA6/23.3% PP–MAV nanocomposite alloy is shown in Figure 10. Only one transition temperature (i.e., T_g) is observed, and this value corresponds to the PA6 phase within the 76.7% PA6/23.3% PP–MAV nanocomposite alloy. The T_g of the PP phase cannot be detected by DSC or by DMA within the examined temperature range. Apparently, the T_g of PA6 increases considerably with the incorporation of PP–MAV nanocomposite. This result is probably because of the relatively high loading and nanoscale size of vermiculite.

The 5% loss temperatures ($T_{-5\%}$) and the maximum weight loss temperatures (T_{max}) determined by DTG are also listed in Table III. It can be seen that the addition of 2–4 wt % vermiculite leads to a dramatic increase in $T_{-5\%}$ from 320.3 to 379.8 °C. Therefore, the $T_{-5\%}$ slightly decreases with further increasing of the vermiculite content. This result demonstrates that the vermiculite addition can greatly improve the thermal stability of PA6. Similarly, the T_{max} of ternary composites tends to increase slightly with the introduction of vermiculite. These data clearly shows the positive

TABLE III
Thermal Properties of PA6/(PP–MAV Nanocomposite) Ternary Composites

Specimen	Vermiculite content, wt %	T_g, °C[a]	T_m^{PP}, °C[b]	T_m^{PA}, °C[b]	($T_m^{PA} - T_m^{PP}$), K[b]	$T_{-5\%}$, °C[c]	T_{max}, °C[c]
Neat PA6	0	60.14	—	225.2	—	320.3	451.9
92.8%PA6/7.8%(PP–MAV)	2	60.03	160.4	225.5	65.10	379.8	473.3
84.5%PA6/15.5%(PP–MAV)	4	61.14	164.2	223.9	59.70	379.8	469.7
76.7%PA6/23.3%(PP–MAV)	6	68.55	165.0	223.2	58.20	366.0	470.8
69.0%PA6/31.0%(PP–MAV)	8	68.75	166.3	223.5	57.20	366.3	469.8

[a] Determined by DMA.
[b] Determined by DSC.
[c] Determined by TGA.

effect of vermiculite on improving the thermooxidative stability of PA6.

CONCLUSIONS

Exfoliated PP–vermiculite nanocomposites can be prepared by melt blending of MA-delaminated vermiculite with PP. Compatibilized ternary blends are injection molded from PA6 and PP–vermiculite. A two-phase structure consisting of PP-vermiculite and PA6 results because of a large difference in the melt viscosities between the phase components. PA6 can be reinforced by the rigid PP–vermiculite phase. The absence of vermiculite reflections in the XRD patterns demonstrates that the PP–vermiculite phase exhibits nanocomposite characteristics. Static and dynamic mechanical tests show that the moduli of nanocomposites tend to increase with increasing PP–vermiculite content. Static tensile test shows that the tensile strength of composite containing 8 wt % vermiculite is higher than that of PA6. At 2–6 wt % vermiculite contents, the tensile strength of composites is slightly lower than that of PA6 because PP exhibits a lower tensile strength than PA6. The morphologies of ternary blends show the fibril formation of PP–vermiculite phase within the PA6 matrix. The thermal properties of PA6 can be improved greatly by the addition of PP–vermiculite.

References

1. (a) Sato, N.; Kurauchi, T.; Sato, S.; Kamigaito, O. J Mater Sci 1991, 26, 3891. (b) Nair, S.V.; Shiao, M.L.; Garrett, P.D. J Mater Sci 1992, 27, 1085. (c) Malzahn, J.C.; Friederich, K. J Mater Sci Lett 1984, 3, 861. (d) Pecorini, T.J.; Hertzberg, R.W. Polym Eng Sci 1994, 15, 174.(e) Joseph, K.; Pavithran, C.; Brahmakumar, M. J Appl Polym Sci 1993, 47, 1731. (f) Garcia-Ramirez, M.; Cavaille, J. Y.; Dupeyre, D.; Peguy, A. J Polym Sci, Polym Phys Ed 1994, 32, 1437.
2. (a) Wei, X. L.; Zhao, K. F.; Lu, T. J.; Xie, Y. C.; Zhu, Q. New Function Materials; Chinese Chemical Engineering Press: Beijing, 1994; p. 125. (b) Taesler, R.; Wittich, H.; Schulte, K.; Kricheldorf, H.R. J Appl Polym Sci 1996, 61, 783. (c) Kobayashi, M.; Takahashi, T.; Takimoto, J.; Koyama, K. Polymer 1995, 36, 3927. (d) Avella, M.; Martuscelli, E.; Raimo, M.; Partch, R.; Gangolli, S.G.; Pascuci, B. J Mater Sci 1997, 32, 2411. (e) Tjong, S.C.; Meng, Y.Z. Polymer 1999, 40, 1109.
3. (a) Fukushima, Y.; Okada, A.; Kawasumi, M.; Kurauchi, T.; Kamigaito, O. Clay Miner 1988, 23, 27. (b) Cho, J. W.; Paul, D. R. Polymer 2001, 42, 1083. (c) Tjong, S. C.; Meng, Y. Z. Chem Mater 2002, 14, 44–51.
4. (a) Vaia, R. A.; Jandt, K. D.; Kramer, E. J.; Giannelis, E. P. Macromolecules 1995, 28, 8080. (b) Akelah, A.; Salahuddin, N.; Hiltner, A.; Baer, E.; Moet, A. Nanostructured Mater 1994, 4, 965. (c) Chang, J. H.; Seo, B. S.; Hwang, D. H. Polymer 2002, 43, 2969. (d) Pinnavaia, T.J. Science 1983, 220, 365. (e) Mehrotra, V.; Giannelis, E.P. Mater Res Soc Symp Proc 1990, 171, 39. (f) Giannelis, E.P. J Minerals Metals Mater Soc 1992, 44, 28.
5. Giannelis, E. P. Adv Mater 1996, 8, 29.
6. Vaia, R. A.; Ishii, H.; Giannelis, E. P. Chem Mater 1993, 5, 1694.
7. Phillon, J. E.; Thompson, M. E. Chem Mater 1991, 3, 777.
8. Wang, M. S.; Pinnavaia, T. J. Chem Mater 1994, 6, 2216.
9. Kim, G. M.; Lee, D. H.; Hoffmann, B.; Kressler, J.; Stöppelmann, G. Polymer 2001, 42, 1095.
10. Maxfield, M.; Christiani, B. R.; Murthy, S. N.; Tuller, H. U.S. Pat. 5,385,776 (1995).
11. Christiani, B. R.; Maxfield, M. U.S. Pat. 5,747,560 (1998).
12. Kawasumi, M., Hasegawa, N., Kato, M., Usuki, A. Macromolecules 1997, 30, 6333.
13. Liu, L.; Qi, Z.; Zhu, X. J Appl Polym Sci 1999, 71, 1133.
14. Tjong, S. C.; Meng, Y. Z. Polymer 1997, 38, 4609.
15. Tjong, S. C.; Meng, Y. Z. Polymer 1998, 39, 5461.
16. Meng, Y. Z.; Tjong, S. C. Polymer 1998, 39, 99.
17. Tjong, S. C.; Meng, Y. Z. Polymer 1999, 40, 7275.
18. Rittler, H. R. U.S. Pat. 4,952,388 (1990).
19. Burnside, S. D.; Wang, H. C. Chem Mater 1999, 11, 1055.
20. Osman, M. A.; Caseri, W. R.; Suter, U. W. J Colloid Interface Sci 1998, 198, 157–163.
21. Rittler, H. R. U.S. Pat. 4,715,987 (1987).
22. Rittler, H. R. U.S. Pat. 4,826,628 (1989).
23. Tjong, S. C.; Meng, Y. Z. Polym Int 1997, 42, 209–217.
24. Datta, A.;Baird, D. G. Polymer 1995, 36, 505.